

# ACCRETION FLOW DYNAMICS OF MAXI J1836-194 DURING ITS 2011 OUTBURST FROM TCAF SOLUTION

Arghajit Jana<sup>1</sup>, Dipak Debnath<sup>1</sup>, Sandip K. Chakrabarti<sup>2,1</sup>, Santanu Mondal<sup>1</sup>, Aslam Ali Molla<sup>1</sup>  
 argha@csp.res.in, dipak@csp.res.in; chakraba@bose.res.in; santanu@csp.res.in,  
 aslam@csp.res.in

## ABSTRACT

The Galactic transient X-ray binary MAXI J1836-194 was discovered on 29th August 2011. Here we make a detailed study of the spectral and timing properties of its 2011 outburst using archival data of RXTE Proportional Counter Array instrument. The evolution of accretion flow dynamics of the source during the outburst through spectral analysis with Chakrabarti-Titarchuk's two-component advective flow (TCAF) solution as a local table model in XSPEC. We also fitted spectra with combined disk blackbody and power-law models and compared it with the TCAF model fitted results. The source is found to be in hard and hard-intermediate spectral states only during entire phase of this outburst. No soft or soft-intermediate spectral states are observed. This could be due to the fact that this object belongs to a special class of sources (e.g., MAXI J1659-152, Swift J1753.5-0127, etc.) that have very short orbital periods and that companion is profusely mass-losing or the disk is immersed inside an excretion disk. In these cases, flows in the accretion disk is primarily dominated by low viscous sub-Keplerian flow and the Keplerian rate is not high enough to initiate softer states. Low-frequency quasi-periodic oscillations (QPOs) are observed sporadically although as in normal outbursts of transient black holes, monotonic evolutions of QPO frequency during both rising and declining phases are observed. From the TCAF fits, we find mass of the black hole in the range of  $7.5 - 11 M_{\odot}$  and from time differences between peaks of the Keplerian and sub-Keplerian accretion rates we obtain viscous timescale for this particular outburst  $\sim 10$  days.

*Subject headings:* X-Rays:binaries – stars individual: (MAXI J1836-194) – stars:black holes – accretion, accretion disks – shock waves – radiation:dynamics

## 1. Introduction

Compact objects such as neutron stars, black holes, etc. are characterized by electromagnetic radiations emitted from the accretion disks, forms due to the accreting matter supplied by their companions. Some of these objects are transient binaries in nature and are very interesting to study using X-rays as they undergo rapid evolutions in their spectral and timing properties. Several works are present in the literature (see, e.g., Tomsick et al., 2000; McClintock & Remillard, 2006; Debnath et al., 2008, 2013; Nandi et al., 2012; Rao, 2013) to explain variation of timing and spectral prop-

erties of these objects during their X-ray outbursts. It also has been reported by several authors that these objects exhibit different spectral states (for e.g., hard, hard-intermediate, soft-intermediate and soft) during their outbursts (see, Debnath et al., 2013 and references therein). Low frequency quasi-periodic oscillations (QPOs) are often observed in the power-density spectra (PDS) of some of these spectral states (see Remillard & McClintock 2006 for a review). In the literature, many authors (Belloni et al., 2005; Debnath et al., 2013 and references therein) have reported that model extracted physical parameters undergo a hysteresis loop during their spectral evolution through an entire epoch of the outburst of these transient black hole candidates (BHCs).

It is well-known that the emitted spectrum of radiation coming from BHCs is multicolor in nature

<sup>1</sup>Indian Center for Space Physics, 43 Chalantika, Garia St. Rd., Kolkata, 700084, India.

<sup>2</sup>S. N. Bose National Centre for Basic Sciences, Salt Lake, Kolkata, 700098, India.

and contains both nonthermal and thermal components. The thermal component is the multicolor blackbody radiation from the standard Keplerian disk (Shakura & Sunyaev, 1973; Novikov & Thorne, 1973) and the other is the power-law component that originates from a ‘‘Compton’’ cloud (Sunyaev & Titarchuk 1980, 1985), a repository of hot electrons whose thermal energy is transferred to low-energy photons from the standard disk by repeated Compton scatterings to produce high-energy X-rays. In the two-component advective flow (TCAF) solution of Chakrabarti & Titarchuk (1995, hereafter CT95; see also, Chakrabarti, 1997), the so-called ‘*Compton cloud*’ or ‘*hot corona*’ is actually the CENtrifugal pressure supported BOundary Layer (CENBOL) that automatically forms behind the centrifugal barrier due to the pileup of the low viscosity (lesser than critical viscosity) and low angular momentum optically thin matter known as sub-Keplerian (halo) accretion component. An axisymmetric shock (Chakrabarti, 1990, 1996; Ryu et al., 1997) defines the outer boundary of the CENBOL. Okuda et al., (2007) showed that this shock is stable even for non-axisymmetric perturbations. In TCAF another component of the accretion flow is the viscous, optically thick and geometrically thin Keplerian (disk) component which is submerged inside the sub-Keplerian (halo) component. CENBOL being much hotter in general, the Keplerian disk is naturally truncated at the shock location close to the black hole. This Keplerian flow settles down to a standard SS73 disk when cooling is efficient (see, Giri et al. 2015, and references therein).

Recently, after the inclusion of two-component advective flow (TCAF) solution in HEASARC’s spectral analysis software package XSPEC (Arnaud, 1996) as a local additive table model (Debnath, Chakrabarti & Mondal, 2014, hereafter DCM14; Mondal, Debnath & Chakrabarti, 2014a, hereafter MDC14; Debnath, Mondal & Chakrabarti, 2015a, hereafter DMC15; Debnath, Molla, Chakrabarti & Mondal, 2015b, hereafter DMCM15), which requires only five physical parameters (including mass) to fit a spectrum from a BHC, an accurate picture of the accretion flow dynamics around several transient BHCs (e.g., H 1743-322, GX 339-4, MAXI J1659-152) during their X-ray outbursts was obtained. From the TCAF model fitted spectrum one cannot only directly obtain information about instantaneous accretion rates of the two components but also obtain crucial information on shock parameters (instantaneous shock location  $X_s$  and shock strength

$\beta = 1/R$ , where  $R$  is the shock compression ratio) which allow us to estimate frequencies of the dominating QPOs (if observed in PDS; see, DCM14). Various spectral states are observed during an outburst phase of a transient BHC, can be characterized by interesting variations of the *accretion rate ratio* (ARR) and QPOs (shape, frequency,  $Q$  value, and rms%). This motivated us to study the accretion flow dynamics of newly discovered Galactic BHC MAXI J1836-194 during its very first outburst in 2011 with TCAF, particularly because of its very low orbital timescale.

The transient BHC MAXI J1836-194 has a short orbital period of  $< 4.9$  hrs and a low disk inclination angle ( $4 - 15^\circ$ ; Russell et al., 2014). The source located at R.A. =  $18^h 35^m 43.43^s$ , Dec =  $-19^\circ 19' 12.1''$  was first observed simultaneously by SWIFT/BAT and MAXI/GSC on 2011 August 29 (Negoro et al., 2011). Miller-Jones et al. (2011), based on X-ray spectral analysis and observation of a radio jet when a transition from hard to soft state occurs, suggested the source to be a potential BHC. Reis et al. (2012) suggested the source to be a highly rotating BHC with a spin parameter of  $a = 0.88 \pm 0.03$ . VLT optical spectral study of the binary system by Russell et al. (2014) suggests that the mass, and the distance of the source to be  $4 - 12 M_\odot$ ,  $4 - 10$  kpc respectively. They also computed the mass and the radius of the companion donor main sequence star to be  $< 0.65 M_\odot$ , and  $< 0.59 R_\odot$  respectively. On the contrary, Cenko et al. (2011) concluded the companion to be a high-massive Be star on the basis of their optical spectroscopic study and system as a high-mass X-ray binary.

MAXI J1836-194 showed its first X-ray flaring activity on 29th August 2011 (Modified Julian Day, i.e., MJD=55802), which continued for the next  $\sim 2$  months. During this outburst period source was studied extensively in multi-energy bands such as various X-ray (Ferrigno et al., 2012; Reis et al., 2012; Radhika et al., 2014), and radio observatories (Yang et al., 2012; Russell et al. 2013). An evolving radio jet was also observed by Russell et al. (2013). We study timing and spectral properties of the BHC during the entire phase of the outburst using RXTE Proportional Counter Array (PCA) archival data. In the present work we give the TCAF fitted spectral analysis results to study accretion flow dynamics around the BHC during its 2011 outburst and discuss how the ARR values and nature of QPOs (if present) vary with spectral states. We also compare our TCAF model fitted spectral results with that of the combined disk blackbody

(DBB) and power-law (PL) model fitted results.

The *paper* is organized in the following way. In §2, we briefly discuss observation and data analysis procedures using HEASARC’s HeaSoft software package. In §3, we present spectral analysis results using the TCAF solution based *fits* file as a local additive table model in XSPEC. We also fitted spectra with the DBB model plus the PL model and compared analysis results with those of the TCAF fitted spectral results to demonstrate the strength of TCAF fits, to understand different spectral states and their correlation with temporal properties. We show that on some days there are clear indications of unresolved double peaked iron lines. Finally in §4, a brief discussion on the results and concluding remarks are presented.

## 2. Observation and Data Analysis

RXTE/PCA monitored the source two days after its discovery on a daily basis (Strohmayer & Smith 2011) except for a crucial  $\sim 5$  days gap during MJD=55813 – 18 in the rising phase of the outburst. Here we study archival data of 35 observational IDs starting from the first PCA observed day; 2011 August 31 (MJD=55804) to 2011 November 24 (MJD = 55889) using XSPEC version 12.8. To analyze the data we follow standard data analysis technique of the RXTE/PCA instrument as presented in Debnath et al. (2013, 2015a).

For timing analysis we use the PCA *Science Binned* mode (FS3f\*.gz) data with a maximum timing resolution of  $125\mu s$  to generate light curves for well-calibrated Proportional Counter Unit 2 (PCU2; including all six layers) in 2 – 25 keV (0-59 channels) and 2 – 15 keV (0-35 channels). To generate the PDS “powspec” routine of the XRONOS package is used to compute rms fractional variability on 2 – 15 keV light curves of 0.01 sec time bin. To find centroid frequencies of QPOs we fit PDS with Lorentzian profiles and use the “fit err” command to get error limits.

For spectral analysis we use *Standard2* mode Science Data (FS4a\*.gz) of the PCA instrument. The 2.5 – 25 keV background subtracted Proportional Counter Unit 2 (PCU2) spectra are fitted with both the TCAF-based model *fits* file and combined DBB and PL model components in XSPEC. The individual DBB and PL model components fluxes are obtained by using the convolution model ‘cflux’ technique. To achieve the best spectral fits, a Gaussian line of peak energy around 6.5 keV (iron-line emission) is used ex-

cept for the five observations (see, Appendix Table I), where we fitted the data with the *LAOR* model (Laor 1991). We fit the data with line energies at  $\sim 7.1$  keV and with emissivity indices around  $\sim 3.5$  (see, Appendix Table II). Hydrogen column density ( $N_H$ ) was kept frozen at  $2.0 \times 10^{21}$  atoms  $\text{cm}^{-2}$  (Kennea et al., 2011) for absorption model *wabs*. For entire outburst, we also use a fixed 1.0% systematic instrumental error for the spectral analysis. The XSPEC command ‘err’ is used to find 90% confidence ‘+ve’ and ‘-ve’ error values for the model fitted parameters after achieving the best fit based on reduced chi-square value ( $\chi_{red}^2 \sim 1$ ). In Appendix Table I, average values of these two  $\pm$  errors are mentioned in the superscripts of the parameter values. In Appendix Table II, we present TCAF with LAOR model fitted LAOR parameters for five spectra, where LAOR model is found to be more useful to deal with Fe line instead of single Gaussian  $\sim 6.5$  keV.

To fit spectra using the TCAF-based model additive table *fits* file, one needs to supply five model input parameters such as, *i*) black hole mass ( $M_{BH}$ ) in solar mass ( $M_\odot$ ) unit, *ii*) Keplerian accretion rate ( $\dot{m}_d$  in Eddington rate  $\dot{M}_{Edd}$ ), *iii*) sub-Keplerian accretion rate ( $\dot{m}_h$  in  $\dot{M}_{Edd}$ ), *iv*) location of the shock ( $X_s$  in Schwarzschild radius  $r_g = 2GM_{BH}/c^2$ ), *v*) compression ratio ( $R = \rho_+/\rho_-$ , where  $\rho_+$  and  $\rho_-$  are post- and pre-shock densities respectively) of the shock. The model normalization value is a fraction of  $\frac{r_g^2}{4\pi D^2} \sin(i)$ , where ‘ $D$ ’ is the source distance (in 10 kpc unit) and ‘ $i$ ’ is the disk inclination angle. In order to fit a black hole spectrum with TCAF model, we create an additive table model *fits* file (*TCAF.fits*) using theoretical model spectra that are generated by varying five input parameters in the modified CT95 code. Basically the governing equations are taken from CT95 as far as hydrodynamics and radiative transfer is concerned. However, the shock strength and the equation to get shock height were generalized to capture features with wider range of accretion rates (see, DCM14 and DMC15). In this Paper for the spectral analysis of MAXI J1836-194 with the TCAF we keep mass a free parameter and find that it comes out to be in the range of  $7.5 - 11 M_\odot$ .

## 3. Results

Our recent study shows that the accretion flow dynamics around a transient BHC can be well understood by the analysis of the spectral and temporal behaviors of the BHC during its outburst under TCAF model paradigm. Here spectral analysis results based

on the TCAF model are presented. We also compare the DBB model plus the PL model fitted results with that of the TCAF model fitted spectral analysis results. It is to be noted that combined PL and DBB model fitted spectral analysis, only provides gross properties of the accretion disk such as fluxes from different thermal and nonthermal components, where as TCAF model goes one step further. The TCAF model extracts detailed physical flow parameters, such as two types of accretion rates and the Compton cloud properties. Furthermore, transitions between different spectral states are more conspicuous when described in terms of the fitted parameters as we shall also see in the case of the present object. Thus, studying accretion dynamics around BHCs with TCAF solution-based *fits* file provides us a certain definite advantages.

To study the timing and spectral properties of MAXI J1836-194 during its current outburst, RXTE/PCA data for 35 observations spread over the entire period of the 2011 outburst are used. We first studied X-ray count rate variation over the entire outburst phase with PCU2 light curves from all observations in the 2 – 25 keV energy band (see Fig. 1a). From the nature of this outburst profile we may define the source into the class belonging to a *fast-rise and slow-decay* type (FRSD) rather than a complete-outbursting *slow-rise and slow-decay* (SRSD) type such as GRO J1655-40, GX 339-4, etc. (Debnath et al., 2010). QPOs are found for only 14 observations out of total of 35. For spectral study we initially fitted spectra with the combined PL and DBB model components. The spectral model fitted parameters such as DBB temperature ( $T_{in}$  in keV), PL photon index ( $\Gamma$ ) and fluxes from both model components are obtained. All the spectra are then refitted with the current version (v0.3) of our TCAF model *fits* file in XSPEC to extract the accretion flow parameters such as Keplerian disk rate ( $\dot{m}_d$ ), sub-Keplerian halo rate ( $\dot{m}_h$ ), shock location ( $X_s$ ) and the compression ratio ( $R$ ) of the shock.

### 3.1. Spectral Analysis with the TCAF Solution and with Combined DBB and PL models

Spectral fit with the conventional DBB plus PL model, which provides us with a rough estimate of the flux contributions coming from both nonthermal (from PL) and thermal (from DBB) processes around a BH. It gives us an rough idea about the evolution of spectral states by monitoring variations of  $T_{in}$ ,  $\Gamma$  factors, and flux contribution from both model components. However, variations of the TCAF fitted/derived parameters

(such as two types of accretion rates,  $\dot{m}_d$  and  $\dot{m}_h$ ; shock parameters,  $X_s$  and  $R$ ; and ARR) provide us with a clear picture of the geometry and the accretion flow dynamics around the BH during the outburst phase. In Appendix Table I, all these spectral fitted/derived parameters are mentioned in a tabular form with estimated errors in superscript. Most importantly, since the entire flow dynamics is determined by these few parameters only, we do not need to change the normalization constant from day to day. The uncertainty in normalization merely reflects the uncertainty in mass measurements.

Figures 1-4 show variations of QPO frequencies, X-ray intensities, and spectral (with DBB plus PL model components and the TCAF model) fitted and derived parameters. In Figure 1a, variation of the background subtracted PCU2 count rate in 2 – 25 keV energy band with time (day in MJD) is shown. In Figure 1c, variation of TCAF model fitted total accretion rates ( $\dot{m}_d$  plus  $\dot{m}_h$ ) in the energy band of 2.5 – 25 keV are shown. To compare with PCU2 rates and with total accretion rates in Figure 1b, total flux variation of the DBB plus PL model fitted spectra of 2.5 – 25 keV are shown. Here we observe that the variation of the TCAF fitted total flow rate (Fig. 1c) is different from the count rate or total flux variations in Figs. 1(a-b) especially in early stages of the outburst. In Fig. 1d, variation of *accretion rate ratio* i.e., ARR (defined as the ratio between sub-Keplerian halo rate with Keplerian disk rate, i.e.,  $\dot{m}_h/\dot{m}_d$ ) is shown. In Fig. 1e, we show QPO frequencies (only dominating primary) with day (in MJD). From the variations of these physical flow parameters, QPO frequencies, etc., only two spectral classes such as *hard* (HS), and *hard-intermediate* (HIMS) are observed during the entire phase of the current outburst of MAXI J1836-194. Note that softer states such as *soft-intermediate* (SIMS), and *soft state* (SS) are absent in contrast to what most of the other outburst sources exhibited (see, e.g., Nandi et al., 2012; Debnath et al., 2013). A similar result of no SS was observed by Debnath et al. (2015b) for another MAXI source, namely MAXI J1659-152 (during its 2010 outburst). The sequence in the present source appears to be: HS (rising) → HIMS (rising) → HIMS (declining) → HS (declining).

In Figs. 2(a-b), variation of DBB temperature ( $T_{in}$  in keV) and power-law photon index ( $\Gamma$ ) with day (MJD) are shown. In Figs. 2(c-d), TCAF model fitted shock location ( $X_s$  in  $r_g$  unit) and compression ratio ( $R$ ) are plotted with day (in MJD). In Figs. 3(a-b),

variations of DBB flux from DBB plus PL model fits and TCAF model fitted Keplerian disk rate with day (MJD) are compared. Similarly, in Figs. 3(c-d), we compare variations of PL flux with sub-Keplerian halo rate from these respective models. Clearly, one can observe ‘some’ similarities in each pair of these compared quantities, but not totally since the PL flux is a function of the disk rate as well.

Figure 4 shows plots of (a) hardness intensity diagram and of (b) ARR and 2 – 15 keV PCU2 count rate is drawn to find a correlation between temporal and spectral properties of the BHC and judge their behavior vis-a-vis classifications. There is clearly a hysteresis behavior. This will be discussed in detail in §3.3. In Fig. 5, TCAF model fitted combined spectra (top panel) and residuals for four spectra of observation Ids: 96371-03-03-01 (MJD=55808.34, black online), 96438-01-01-04 (MJD=55818.85, red online), 96438-01-02-04 (MJD=55823.82, blue online), and 96438-01-06-02 (MJD=55850.87, orange online), selected from different regions i.e., states of the outburst are shown. Here (i), and (iv) plots are for hard states of and plots (ii), and (iii) are for hard-intermediate states of rising and declining phases respectively. We observe that in (i) and (iii) the fits are better with an additional *LAOR* model described iron line component which appears to be unresolved double lines (Fabian et al. 1989; Stella 1990). In (ii) and (iv) we required only a single Gaussian to model the single iron lines.

To check correlation among spectral fitted parameters, in Fig. 6(a-d), we make comparative plots of *i*) total (DBB plus PL) flux vs. total flow rate ( $\dot{m}_d$  plus  $\dot{m}_h$ ), *ii*) ARR vs. QPO frequency, *iii*)  $\dot{m}_h$  vs.  $\dot{m}_d$ , and *iv*) PL photon index  $\Gamma$  vs.  $\dot{m}_h$ . In Fig. 6a, correlation is expected. In Fig. 6b, no correlation is expected in any obvious sense and the QPOs are related to resonance effects between cooling timescale (a function of  $\dot{m}_h$  and  $\dot{m}_d$ ) and infall timescale (a function of  $X_s$  and  $R$ ). In Fig. 6c, weak coupling between the two rates ( $\dot{m}_h$  and  $\dot{m}_d$ ) is due to the fact that at least a fraction of the disk rate is the bi-product of the halo rate mediated by viscosity. In Fig. 6d, a weak coupling of rising of  $\Gamma$  with  $\dot{m}_h$  was expected even from the basic work of CT95 when  $\dot{m}_d$  is almost constant and small. We made statistical analysis using two correlation methods such as Spearman Rank (SR) and Pearson Linear (LP), and found that total fluxes are strongly correlated with total accretion rates (SR coefficient  $SR_e=0.964$ , LP coefficient  $LP_e=0.976$ ), no or weak anti-correlation between ARR and QPO frequency ( $SR_e=-0.008$ ,  $LP_e=-0.363$ ),

and a weak correlation between two types ( $\dot{m}_h$ , and  $\dot{m}_d$ ) of accretion rates ( $SR_e=-0.336$ ,  $LP_e=-0.418$ ), and PL photon index  $\Gamma$  with halo ( $\dot{m}_h$ ) rate ( $SR_e=0.271$ ,  $LP_e=0.221$ ). We also find that  $\Gamma$  and ARR are weakly anti-correlated with each other ( $SR_e=-0.278$ ,  $LP_e=-0.404$ ) as expected from the argument given above.

### 3.2. Evolution of Spectral and Temporal Properties during the Outburst

The spectral and temporal properties of this object during its first outburst are discussed by several authors on the basis of X-ray or radio variability, QPO observations, spectral results based on inbuilt XSPEC model fits, such as, thermal DBB and nonthermal PL components (Ferrigno et al. 2012; Radhika et al. 2014; Russell et al. 2014). However, spectral fits on a daily basis with TCAF provides us with a variation of physical parameters and enlighten us with physical reason behind different spectral states observed during the outburst. It also allows us to find a pattern to correlate with spectral transitions and their sequences. Recently, interesting correlations in 2010 outburst of H 1743-322 (MDC14), in 2010-11 outburst of GX 339-4 (DMC15) and in 2010 outburst of MAXI J1659-152 (DMCM15) were found. It was observed that two-component accretion rates ( $\dot{m}_d$ ,  $\dot{m}_h$ ), ARRs, shock locations, and compression ratios in conjunction with observed QPOs provided a better characterization of the classification of spectral states. The nature of different spectral states observed during the 2011 outburst of MAXI J1836-194 will be discussed below in the sequence of their appearance.

*(i) Hard State (Rising phase):* RXTE started observing the source two days after its discovery. The source is observed in the hard state for the first  $\sim 7$  days of the observation (from MJD = 55804.52 to 55810.29). Low values of the observed power-law photon indices (between  $\sim 1.65 - 1.75$ ) allow us to conclude that the object is in the hard state. PCA count rate, total flow/accretion rates increase with time (day) and reach their individual maximum observable values on the transition (HS to HIMS) day (MJD=55810.29), when a local maximum of ARR and sub-Keplerian halo rate ( $\dot{m}_h$ ) are also observed (see Figures 1 & 3). QPOs are observed only for two observations during this phase and the frequencies increased as in normal outburst, indicating that the underlying shocks whose oscillations cause QPOs may be moving inward but the resonance condition (that cooling and infall timescales should be close to each other) is not satisfied on some days. One

reason for this may be that the ARR is almost constant (see, Mondal et al., 2015, and Chakrabarti et al., 2015 for more details). Another reason may be that there are excess sub-Keplerian halo matter coming from the companion which is not a part of the accretion process that surrounds the system as a whole. It is also possible that the companion is a Be star and the accretion disk is immersed inside the excretion disk, a fact borne out by generally very low values of spectral indices in hard state spectra signifying the presence of a ‘super-hard’ state. The flux is also maximum in this state, which is unusual as the flux is generally highest in the soft/soft-intermediate states that are missing for this outburst of the source (see, Debnath et al., 2008, 2013; Nandi et al., 2012).

We classify HIMS into two parts, HIMS (rising) and HIMS (declining), since there is a sharp change of physical (both temporal and spectral) properties on a day that is termed as the transition day. On this day QPO frequency was found to be the highest.

(ii) *Hard-Intermediate State (Rising phase)*: This state lasts for  $\sim 10$  days. ARR decreases monotonically due to rise in  $\dot{m}_d$  and fall in  $\dot{m}_h$ . At the same time, PL  $\Gamma$  increases monotonically and DBB  $T_{in}$  decreases. This may be because of more supply of matter from thermally cooler Keplerian disk component as viscosity rises. On the transition day (MJD=55820.41). The ARR is found to have its lowest value with a maximum in  $\dot{m}_d$  and a minimum in  $\dot{m}_h$ . During this phase, QPO is observed on only three days. QPO frequency continues to increase. This behavior may also be due to the same reason as that of the rising HS stated above.

(iii) *Hard-Intermediate State (Declining phase)*: For the next  $\sim 11$  days starting from the transition day when the QPO frequency has the maximum value, source was in this spectral state. During this phase, QPOs are observed sporadically though the frequency monotonically decreased from 5.175 to 2.023 Hz within the first  $\sim 9$  days of this state. ARR is found to increase rapidly with a rise in halo rate and decrease in disk rate (see Figure 1 and 3). This causes a rapid decrease in  $\Gamma$  also indicates that spectrum start to become harder from the first day of this state. On September 27 (MJD=55831.85), transition from declining hard-intermediate to hard spectral state was seen as on this particular day and a local maximum in the ARR is also observed. A similar nature was found on the rising hard to hard-intermediate transition day. Precisely this behavior was seen in our earlier study on other transient BHCs with the TCAF fits as well (see,

MDC14, DMC15, DMCM15).

(iv) *Hard State (Declining phase)*: The source is found to be in this spectral state until the end of our observation (MJD=55889.16) starting from the HIMS-HS transition day. In this phase of the outburst, supply from both components of matter is cut off as a result of that the ARR values decreasing steadily with time (day). Shock recedes back as day progresses with a slow rise in compression ratios. QPOs are observed sporadically during only three observations with the frequency decreasing monotonically. On other days the resonance condition was not fulfilled and QPOs were not observed. Note the unusually low value of the spectral index. This could be because the entire disk system is immersed in an excretion disk or winds of the companion. This is also a reason why QPOs are not observed regularly everyday as in the same states of other outburst sources.

### 3.3. ARR-Intensity Diagram (ARRID): A Correlation Between Timing and Spectral Properties

In Fig. 4(a-b), we showed evolution of various quantities during the entire outburst to impress that the parameters of the declining phase do not retrace themselves during the rising phase. In the so-called hardness-intensity (HID) diagram, data are plotted mainly using photon counts from light curves in selected constant energy ranges throughout the outburst and one tries to find correlation. Sometimes the curve looks like a ‘q’ and the diagram is called q-diagram (Maccarone & Coppi, 2003; Fender et al., 2004; Belloni et al., 2005). In Fig. 4a, the HID diagram is drawn. Days when state transitions occur are not obvious. Since state transitions are necessarily due to accretion rate variations (CT95), it is instructive to make a plot with physical parameters where transitions of states are obvious from the diagram itself. In Fig. 4b, we plot the variation of the 2 – 25 keV PCU2 count rate as a function of ARR ( $\dot{m}_h/\dot{m}_d$ ). We define it as the *accretion rate ratio intensity diagram* (ARRID). Here B, C, and D represent the days when state transitions took place and points A, and E mark start and end of the observation. It clearly shows a hysteresis effect and different branches are associated with different spectral states. A-B (black online), D-E (violet online) represent HS in rising and declining phases respectively. The points B and D mark transition days between HS and HIMS, when ARR acquires local maximum value, irrespective of the count rate.

The point C marks the transition day between two HIMS, when a sharp change in physical (spectral and temporal) properties, such as minimum ARR and maximum QPO frequency, etc. are observed, irrespective of PCU2 count rate. The approximate horizontal lines, B-C (red online) and C-D (green online) represent HIMS in rising and declining phases respectively.

#### 4. Discussions and Concluding Remarks

We study the evolution of the spectral and temporal properties of a Galactic transient BHC MAXI J1836-194 during its first (2011) X-ray outburst using RXTE PCU2 data. For spectral evolution study, we use two models (TCAF and DBB plus PL models) applied to a total of 35 observations. A combined PL and DBB model fit provides us with a rough estimate of thermal (DBB) and nonthermal (PL) flux contributions as well as an idea about the disk temperatures ( $T_{in}$ ) and PL photon indices ( $\Gamma$ ). The TCAF model (v0.3) fit provides us with physical accretion flow parameters such as the Keplerian disk ( $\dot{m}_d$ ), sub-Keplerian halo ( $\dot{m}_h$ ) rates, the shock location ( $X_s$ ), and the shock compression ratio ( $R$ ; see, Figures 1-3). In Appendix Table I, a detailed spectral analysis results with observed QPO frequencies are presented. The variation of these model fitted parameters with the ARR (a ratio between  $\dot{m}_h$  to  $\dot{m}_d$ ), and properties of QPOs (if observed) provide us with a better understanding of the accretion flow dynamics around the BHC during its outburst.

So far we have successfully studied the accretion flow dynamics of three Galactic BHCs (H 1743-322, GX 339-4, and MAXI J1659-194) during their X-ray outbursts from our spectral study with the TCAF model (see MDC14, DMC15, DMCM15). A strong correlation between spectral and timing properties are found for these sources giving rise to transitions between different spectral states. Generally four (HS, HIMS, SIMS, and SS) spectral states are observed during an outburst of transient BHC in the sequence of HS→HIMS→SIMS→SS→SIMS→HIMS→HS. According to CT95, Ebisawa et al., (1996), an outburst of transient BHCs is triggered due to a sudden rise in viscosity at the outer edge of the disk and the declining phase begins when the viscosity is turned off at the outer edge (CT95; Ebisawa et al., 1996). If viscosity does not rise above a critical value (Chakrabarti, 1990), the Keplerian component does not form and as a result we may miss soft states (SS) altogether during an outburst (DMCM15). The resulting event could be

termed as a ‘failed’ outburst.

The QPOs (generally type ‘C’) are found to evolve monotonically in rising/declining hard and hard-intermediate spectral states (Chakrabarti et al., 2005, 2008; Debnath et al., 2010, 2013; Nandi et al., 2012). We also observed a local maximum of ARR on the transition day of HS  $\rightleftharpoons$  HIMS and of evolving QPO frequency on HIMS  $\rightleftharpoons$  SIMS transition day (MDC14, DMC15, DMCM15). QPOs are observed sporadically on and off during SIMS and are absent in SS (Debnath et al., 2008, 2013; Nandi et al., 2012). During the rising hard state, the ARR is found to increase monotonically with a rise in the halo rate and reaches its maximum on the HS-HIMS transition day and the shock is found to move in gradually weakening its strength. In rising HIMS the shock further moves in rapidly due to shrinking of the CENBOL size. This may be due to the rapid rise in the thermally cooler Keplerian disk rate, which reaches maximum on HIMS-SIMS transition day. Also, on the transition day, shock compression ratio ( $R$ ) becomes approximately unity. During this process the ARR rapidly reduces to a lower value on the transition day. During rising SIMS, ARR are observed at a lower value with very little variation and generally type B or A QPOs are observed sporadically. The origin of these QPOs is assumed to be different and may be due to non-satisfaction of Rankine-Hugoniot condition to form a stable shock location (Ryu et al., 1997; Chakrabarti et al., 2015). A strong jet may be found during this phase of the outburst that may be due to the cooling down of the base of the CENBOL with a sudden rise in the Keplerian matter contributions. The cooling reduces sound speed, making the upper part of the jet become supersonic quite abruptly. In the soft state the ARR reduces further with a clear dominance of the Keplerian component. In the declining SIMS the contribution of the Keplerian component starts to decrease and sporadic appearances of QPOs are seen. The ARR varies in a similar way as of rising SIMS. On the declining SIMS-HIMS transition day the maximum value of the QPO frequency could be found. In the process, during the declining HIMS the ARR rises rapidly and reaches its maximum value on the HIMS-HS transition day. QPO frequencies are observed to decrease continuously in a rapid manner with an outward movement of the shock and a rise in compression ratios. In the declining hard state, both ARR and QPO frequency decrease with time with a rapid outward movement of shock. At the same time a decrease in both components of accretion rates could

be observed.

The present analysis of the outburst data reveals a great deal of surprises. Depending on the nature of the variation of the TCAF model fitted or derived parameters ( $\dot{m}_d$ ,  $\dot{m}_h$ , ARR,  $X_s$ , R, etc.), and nature of the QPOs (if present), only two spectral classes, namely, *hard* (HS), and *hard-intermediate* (HIMS), are observed during the entire phase of the current outburst of MAXI J1836-194. These spectral states are observed in the sequence of: HS (rising)  $\rightarrow$  HIMS (rising)  $\rightarrow$  HIMS (declining)  $\rightarrow$  HS (declining). The so-called ‘q’-diagram does not show a ‘q’ shape at all (see, Fig. 4a). In the ARRID diagram (Fig. 4b), the evolution of the 2 – 25 keV PCU2 count rate with the ARR, which hints at a hysteresis behavior, strongly justifies our spectral classification. Different branches of the plot appear to be related to different spectral states. We clearly see that the ARR has a local maximum on transition days of HS  $\rightleftharpoons$  HIMS. This plot provides us with a better understanding of the strong correlation between spectral and temporal properties. In MDC14, a similar type of correlation between different spectral states was also found for Galactic BHC H 1743-322 during its 2010 outburst.

A peculiarity of this outburst of MAXI J1836-194 is that QPOs are not seen every day, although there is a general trend similar to other outbursts: increasing of frequency during the rising phase and decreasing of frequency in the declining phase of the outburst. Also, we have not found any signature of the soft and soft-intermediate spectral states. The source started and ended from/to hard spectral states via two hard-intermediate spectral states during the entire phase of the outburst. Furthermore, the spectral indices in few observation of hard states are very low (i.e., spectra are super-hard). The unusual behavior of the source during this outburst may be due to a shorter orbital period of the binary system which makes the disk very small in size and it is possibly immersed in the wind or the excretion disk of the companion; this would be the case if the companion is a Be Star, for instance (Cenko et al., 2011). During most of this outburst the source was covered with low angular momentum matter which is not necessarily a part of the accretion disk. The non-observation of QPOs on a regular basis is also explained since resonance condition for QPOs would be difficult to fulfill in the presence of such extraneous matter (see, Molteni et al., 1996; Mondal et al., 2015; Chakrabarti et al., 2015) which are not included in the TCAF solution.

For a detailed analysis of the TCAF parameters, one may be able to estimate the viscous timescale using time differences between peaks of the Keplerian disk and sub-Keplerian halo component rates during rising or declining phases of an outburst of a transient BHC. MAXI J1836-194 shows double humps for both of the accretion rates during the entire phase of the current outburst. During the rising phase the halo rate attains its maximum value on MJD=55810, whereas the disk rate attains its peak after  $\sim 10$  days when the halo reaches its first minimum. Again, during the declining phase the halo rate starts to increase and attains its second peak on MJD=55826. At the same time the disk rate attains its second peak on MJD=55836, which is coincidentally exactly after  $\sim 10$  day interval. The observed time gaps between the peaks of  $\dot{m}_h$  and  $\dot{m}_d$  in both the rising and declining phases suggests that the viscous timescale of MAXI J1836-194 during 2011 outburst could be around of  $\sim 10$  days.

Recently, Shaposhnikov & Titarchuk (2009) have found that the scaling method of PL photon Index ( $\Gamma$ ) vs. QPO frequency diagram is a powerful tool to predict mass of an unknown BHC. For that, one needs sufficient number of observations, especially at the bending and horizontal saturation branches of the diagram. This method is not useful to predict the mass of the current BHC MAXI J1836-192, since there are only two observations of QPOs (4.35 and 5.17 Hz) at the saturation level, and no QPOs in the region where the slope turns into the saturation level for higher frequencies and indices. So we obtain the mass of the unknown BH from our TCAF fits.

To further emphasize the advantage of the TCAF fits, we wish to emphasize that the model normalization is the normalization of the whole spectrum that it arises out of the difference between the calculated spectrum at the disk frame and the observer’s frame which includes the idiosyncrasies of the instruments. Once the spectrum is calculated using certain inner edges and other parameters there is no way that a normalization constant should contain the disk parameters anymore. Strangely, our precision fitting with the TCAF model does not require one to vary the normalization constant as in other models. This is because the TCAF solution normalization depends on the source distance ( $D$ ) and the disk inclination angle ( $i$ ), for a given mass of the black hole, all intrinsic properties of the disk (such as the inner edge of the disk) which are used inside normalization in other models are all used up to obtain the spectrum itself. Indeed, we get ex-

cellent fits keeping the normalization constant within a narrow range as it should be for the current source MAXI J1836-194 and the source MAXI J1659-152 during its 2010 outburst (Molla et al. 2016). On the other hand, the normalization required for DBB varies from day to day. These are given in Appendix Table I. This nonconstancy has been variously explained by the change of the inner edge of the disk, which we find intriguing since the truncated disk information should have already been used to fit the data in the first place. Our model normalization is found to vary in a narrow range of 0.25 – 0.35, (DBB model normalization shows wild variation in the range of 0.34 – 291) except for five observations around the transition day between two HIMS when a prominent jet is observed (see, Russell et al., 2013). The deviation of the normalization in these days reflects the non-inclusion of contribution from the jet in the current version (v0.3) of the TCAF model *fits* file. During the spectral fitting, as we kept mass of the BH as a free parameter, the  $M_{BH}$  is found in the range of 7.5 – 11  $M_{\odot}$ . The detailed method of the prediction of the BH mass from the TCAF fitting are discussed in Molla et al. (2016).

In the future, we will make detailed spectral and temporal study of other similar short orbital period BHCs (for e.g., XTE J1118+480 of orbital period  $\sim$  4.1 hrs, González-Hernández et al., 2013; Swift J1753.5-0127 of orbital period  $\sim$  3.2 hrs, Zurita et al., 2007) during their X-ray outbursts to check if flow dynamics of these sources also follow a similar trend.

### Acknowledgments

AJ and DD acknowledge support from ISRO sponsored RESPOND project fund (ISRO/RES/2/388/2014-15). DD also acknowledges support from DST sponsored Fast-track Young Scientist project fund (SR/FTP/PS-188/2012). AAM and SM acknowledge supports of MoES sponsored junior research fellowship and post-doctoral fellowship respectively.

### REFERENCES

Arnaud, K.A., 1996, ASP Conf. Ser., Astronomical Data Analysis Software and Systems V, ed. G.H. Jacoby & J. Barnes, 101, 17

Belloni, T., Homan, J., Casella, P., et al., 2005, A&A, 440, 207

Chakrabarti, S. K., 1990, “Theory of Transonic Astrophysical Flows”, World Scientific (Singapore)

Chakrabarti, S.K., & Titarchuk, L.G., 1995, ApJ, 455, 623 (CT95)

Chakrabarti, S. K., 1996, ApJ, 464, 664

Chakrabarti, S.K., 1997, ApJ, 484, 313

Chakrabarti, S. K., Nandi, A., & Debnath, D., et al., 2005, IJP, 79, 841 (arXiv:astro-ph/0508024)

Chakrabarti, S.K., Debnath, D., & Nandi, A., et al., 2008, A&A, 489, L41

Chakrabarti, S.K., Mondal, S., & Debnath, D., 2015, MNRAS, 452, 3451

Cenko, S. B., Miller, A. A. & Bloom, J. S., 2011, ATel, 3614, 1

Debnath, D., Chakrabarti, S.K., & Nandi, A., et al., 2008, BASI, 36, 151

Debnath, D., Chakrabarti, S.K., & Nandi, A., 2010, A&A, 520, A98

Debnath, D., Chakrabarti, S.K., & Nandi, A., 2013, AdSpR, 52, 2143

Debnath, D., Mondal, S., & Chakrabarti, S.K., 2014, MNRAS, 440, L121 (DCM14)

Debnath, D., Mondal, S., & Chakrabarti, S.K., 2015a, MNRAS, 447, 1984 (DMC15)

Debnath, D., Molla, A.A., Chakrabarti, S.K., & Mondal, S., 2015b, ApJ, 803, 59 (DMCM15)

Ebisawa, K., Titarchuk, L.G., & Chakrabarti, S.K., 1996, PASJ, 48, 59

Fabian, A. C., Rees, M. J., Stella, L., & White, N. E., 1989, MNRAS, 238, 729

Fender, R. P., Belloni, T. M., & Gallo, E., 2004, MNRAS, 355, 1105

Ferrigno C., Bozzo, E. & Del S., et al., 2012, A&A, 537, L7

González-Hernández, J. I., Rebolo, R. & Casares, J., 2013, Proc. of hsa7.conf, 561

Giri, K., Garain, S. & Chakrabarti, S.K., 2015, MNRAS, 448, 3221

- Kennea, J. A., Hoversten, E. A., & Siegel, M. H., et al., 2011, *ATel*, 3613, 1
- Laor, A., 1991, *ApJ*, 376,90
- Maccarone, T. J. & Coppi, P. S., 2003, *MNRAS*, 338, 189
- McClintock, J. E., & Remillard, R. A., 2006, in *Compact Stellar X-ray Sources*, ed. W. Lewin & M. van der Klis, 39, 157
- Miller-Jones, J. C. A., Sivakoff, G. R., & Rupen, M., et al., 2011, *ATel*, 3628, 1
- Molla, A. A., Debnath, D., & Chakrabarti, S. K., et al., 2016, *MNRAS* (submitted)
- Molteni, D., Sponholz, H., & Chakrabarti, S.K., 1996, *ApJ*, 457, 805
- Mondal, S., Debnath, D., & Chakrabarti, S.K., 2014a, *ApJ*, 786, 4 (MDC14)
- Mondal, S., Chakrabarti, S.K., & Debnath, D., 2014b, *Ap&SS*, 353, 223
- Mondal, S., Chakrabarti, S.K., & Debnath, D., 2015, *ApJ*, 798, 57
- Nandi, A., Debnath, D., Mandal, S., & Chakrabarti, S.K., 2012, *A&A*, 542, A56
- Negoro, H., Nakajima, M. & Nakahira, S., et al., *ATel*, 3611, 1
- Novikov, I., & Thorne, K.S., 1973, in *Black Holes*, Ed. C. DeWitt & B.S. DeWitt (New York: Gordon & Breach), 343
- Okuda, T., Teresi, V. & Molteni, D., 2007, *MNRAS* 377, 1431
- Radhika, D., Ramadevi, M. C. & Seetha, S., *ApJ* (submitted) (arXiv: 1401.1135)
- Rao, A. R., 2013, *ASI Conf. Ser.*, Ed. S. Das, A. Nandi & I. Chattopadhyay, 8, 63
- Reis R. C., Miller, J. M., Reynolds, M. T., et al., 2012, *ApJ*, 751, 34
- Remillard, R.A., & McClintock, J.E., 2006, *ARA&A*, 44, 49
- Ryu, D., Chakrabarti, S.K., & Molteni, D., 1997, *ApJ*, 474, 378
- Russell, D. M., Russell, T. D., & Miller-Jones, J. C. A., et al., 2013, *ApJ*, 768, 35
- Russell, T. D., Soria, R., & Miller-Jones, J. C. A., et al., 2014, *MNRAS*, 439, 1390
- Shakura, N.I., & Sunyaev, R.A., 1973, *A&A*, 24, 337 (SS73)
- haposhnikov, N. I. & Titarchuk, L., 2009, *ApJ*, 699, 4535
- Stella, L., 1990, *Nature*, 334, 747
- Strohmer, T. E. & Smith, E. A., 2011, *ATel*, 3618, 1
- Sunyaev, R.A., & Titarchuk, L.G., 1980, *ApJ*, 86, 121
- Sunyaev, R.A., & Titarchuk, L.G., 1985, *A&A*, 143, 374
- Tomsick, J. A., Kaaret, P., Kroeger, R. A., & Remillard, R., 2000, *ApJ*, 512, 892
- Yang, J. Xu, Y. & Li, Z., et al., *MNRAS*, 426, L66
- Zurita, C., Torres, M.A.P., Durant, M., et al., 2007, *ATel*, 1130, 1

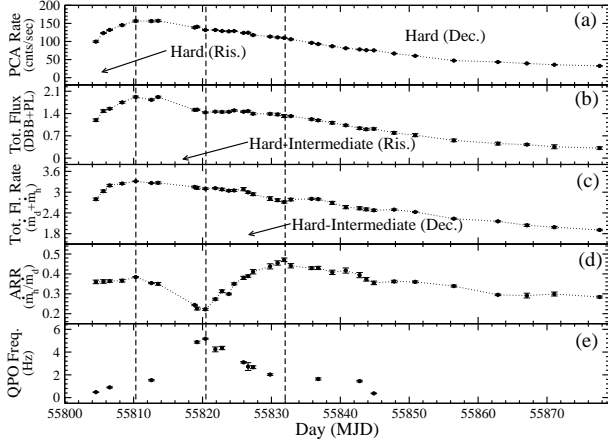


Fig. 1.— Variation of (a) 2 – 25 keV PCA count rates (cnts/sec), (b) combined disk black body (DBB) and power-law (PL) model fitted total spectral flux in 2.5 – 25 keV range (in units of  $10^{-9} \text{ ergs cm}^{-2} \text{ s}^{-1}$ ), (c) TCAF model fitted total flow (accretion) rate (in  $\dot{M}_{Edd}$ ; sum of Keplerian disk,  $\dot{m}_d$  and sub-Keplerian halo  $\dot{m}_h$  rates) in the 2.5 – 25 keV energy band, and (d) accretion rate ratio (ARR; ratio between halo and disk rates) with day (MJD) for the 2011 outburst of MAXI J1836-194 are shown. In the bottom panel (e), observed primary dominating QPO frequencies (in Hz) with day (MJD) are shown. The vertical dashed lines indicate transitions between different spectral states.

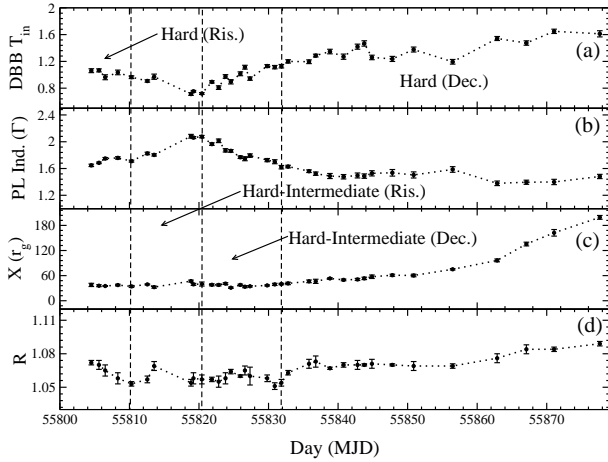


Fig. 2.— Variation of combined DBB and PL model fitted (a) disk temperature  $T_{in}$  (in keV), and (b) PL photon index ( $\Gamma$ ) with day (MJD) are shown in top two panels. Variations of TCAF model fitted/derived (c) shock location ( $X_s$  in  $r_g$ ) and (d) compression ratio ( $R$ ), with day (MJD) are shown.

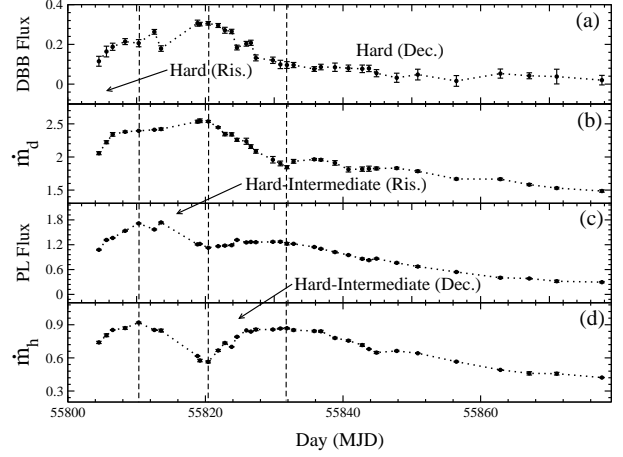


Fig. 3.— In top panel (a), the variation of combined disk black body (DBB) and power-law (PL) model fitted DBB spectral flux and in panel (c), the variation of PL spectral flux (both in units of  $10^{-9} \text{ ergs cm}^{-2} \text{ s}^{-1}$ ) in 2.5 – 25 keV energy range are shown. In panel (b), the variation of TCAF model fitted Keplerian disk rate  $\dot{m}_d$  and in bottom panel (d), the variation of sub-Keplerian halo rate  $\dot{m}_h$  (both in  $\dot{M}_{Edd}$ ) in the same energy band are shown.

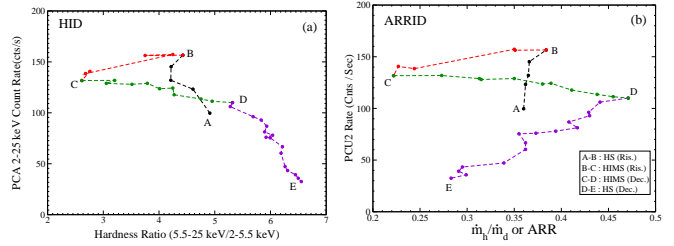


Fig. 4.— (a) Hardness (ratio between 5.5 – 25 keV to 2 – 5.5 keV PCU2 count rates)-Intensity diagram for the entire 2011 outburst of MAXI J1836-194. Note that the 'q' shape (for e.g., Belloni et al., 2005) is not formed in this case. (b) Evolution of 2 – 15 keV PCA count rate as a function of ARR ( $\dot{m}_h/\dot{m}_d$ ), showing the hysteresis effect. Transitions from HS to HIMS (rising) and the reverse (declining) take place when ARR is local maximum.

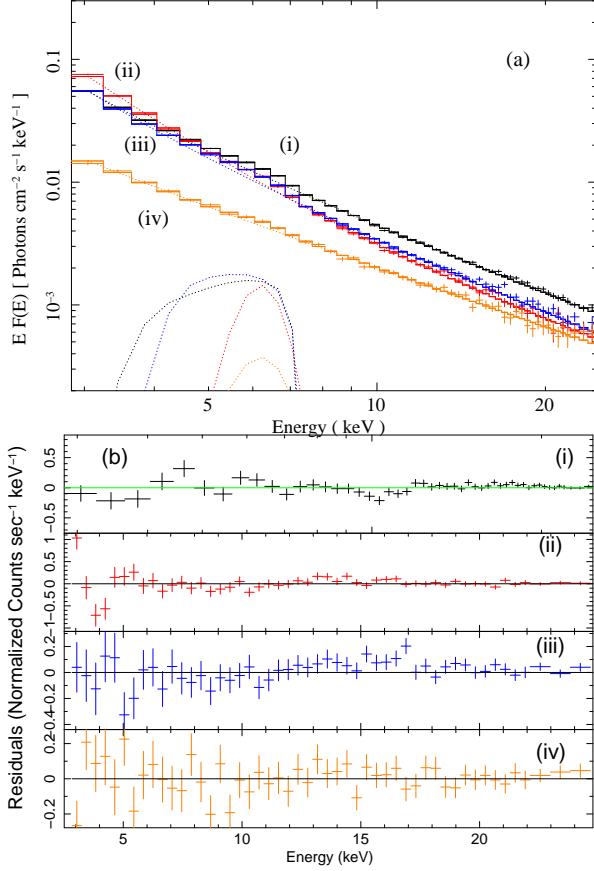


Fig. 5.— In left panel (a), TCAF model fitted spectra for (i) HS (Ris.), (ii) HIMS (Ris.), (iii) HIMS (Dec.), and (iv) HS (Dec.) for observations Ids : 96371-03-03-01 (MJD=55808.34), 96438-01-01-04 (MJD=55818.85), 96438-01-02-04 (MJD=55823.82), and 96438-01-06-02 (MJD=55850.87) respectively. In plots (i) & (iii) we use an additional LAOR component and in (ii) & (iv) a Gaussian Fe emission line are used to fit the spectra. Observed data (points with error bars) and combined models (solid histogram) are shown in the plots. In the right panel (b), model fitted residual plots are shown. The parameters of the fits are listed in Appendix Table I.

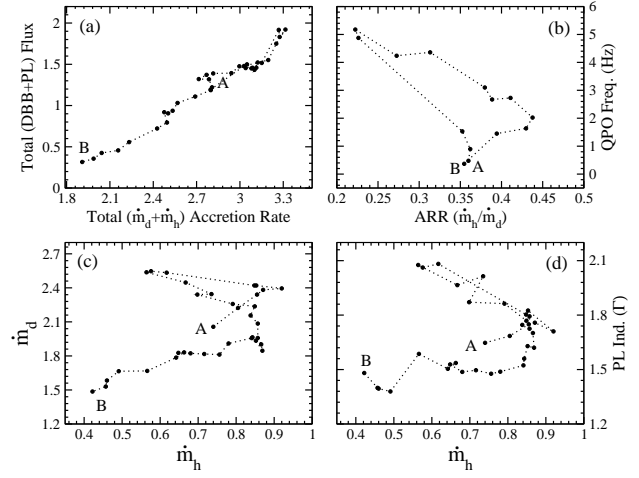


Fig. 6.— Comparative plots between (a) total flow ( $\dot{m}_d$  plus  $\dot{m}_h$ ) rates vs. total (DBB plus PL) flux, (b) ARR vs. QPO frequencies, (c)  $\dot{m}_h$  vs.  $\dot{m}_d$  rates, and (d)  $\dot{m}_h$  rates vs. PL photon indices. Note: here points A, and B are mark start and end of our observations.

## Appendix I

2.5-25 keV Combined DBB plus PL and TCAF Model Fitted Spectral Parameters with QPOs

Obs. Id	MJD	$T_{in}$ (keV)	$\Gamma$	$DBBf^\dagger$	$PLf^\dagger$	DBB Norm.	$\dot{m}_d$ ( $M_{Edd}$ )	$\dot{m}_h$ ( $M_{Edd}$ )	ARR	$X_s$ ( $r_g$ )	R	Norm.	$M_{BH}$ ( $M_\odot$ )	QPO <sup>††</sup> (Hz)	$\chi^2/DOF$
(1)	(2)	(3)	(4)	(5)	(6)	(7)	(8)	(9)	(10)	(11)	(12)	(13)	(14)	(15)	(16)
X-01-00*	55804.52	1.061 <sup>0.029</sup>	1.647 <sup>0.018</sup>	0.115 <sup>0.025</sup>	1.078 <sup>0.012</sup>	11.27 <sup>1.38</sup>	2.057 <sup>0.023</sup>	0.740 <sup>0.010</sup>	0.360 <sup>0.009</sup>	37.84 <sup>3.820</sup>	1.072 <sup>0.017</sup>	0.341 <sup>0.002</sup>	10.49 <sup>0.22</sup>	0.476 <sup>0.027</sup>	61.33/41
X-02-00*	55805.61	1.066 <sup>0.023</sup>	1.685 <sup>0.012</sup>	0.164 <sup>0.027</sup>	1.315 <sup>0.014</sup>	15.63 <sup>1.62</sup>	2.223 <sup>0.023</sup>	0.805 <sup>0.013</sup>	0.362 <sup>0.010</sup>	35.93 <sup>2.230</sup>	1.070 <sup>0.004</sup>	0.347 <sup>0.002</sup>	10.91 <sup>0.34</sup>	---	62.41/41
X-03-00**	55806.51	0.963 <sup>0.037</sup>	1.749 <sup>0.015</sup>	0.188 <sup>0.018</sup>	1.364 <sup>0.010</sup>	31.25 <sup>2.46</sup>	2.341 <sup>0.028</sup>	0.853 <sup>0.003</sup>	0.364 <sup>0.007</sup>	35.23 <sup>1.511</sup>	1.065 <sup>0.005</sup>	0.349 <sup>0.027</sup>	10.96 <sup>0.34</sup>	0.895 <sup>0.050</sup>	44.93/38
X-03-01**	55808.33	1.035 <sup>0.035</sup>	1.758 <sup>0.018</sup>	0.214 <sup>0.015</sup>	1.536 <sup>0.011</sup>	23.98 <sup>1.94</sup>	2.380 <sup>0.012</sup>	0.870 <sup>0.011</sup>	0.366 <sup>0.007</sup>	39.00 <sup>2.210</sup>	1.057 <sup>0.005</sup>	0.741 <sup>0.057</sup>	9.99 <sup>0.31</sup>	---	28.58/38
X-03-02*	55810.29	0.964 <sup>0.021</sup>	1.710 <sup>0.015</sup>	0.206 <sup>0.018</sup>	1.715 <sup>0.011</sup>	34.02 <sup>1.98</sup>	2.395 <sup>0.004</sup>	0.920 <sup>0.005</sup>	0.384 <sup>0.003</sup>	34.19 <sup>2.470</sup>	1.053 <sup>0.009</sup>	0.345 <sup>0.076</sup>	10.87 <sup>0.37</sup>	---	65.27/41
X-03-03**	55812.57	0.907 <sup>0.018</sup>	1.825 <sup>0.019</sup>	0.263 <sup>0.012</sup>	1.569 <sup>0.012</sup>	60.71 <sup>1.66</sup>	2.411 <sup>0.004</sup>	0.853 <sup>0.005</sup>	0.354 <sup>0.003</sup>	39.01 <sup>1.118</sup>	1.057 <sup>0.003</sup>	0.542 <sup>0.087</sup>	11.01 <sup>0.27</sup>	1.531 <sup>0.066</sup>	53.50/38
Y-01-00*	55813.55	0.971 <sup>0.039</sup>	1.803 <sup>0.017</sup>	0.179 <sup>0.014</sup>	1.738 <sup>0.013</sup>	280.24 <sup>17.9</sup>	2.421 <sup>0.017</sup>	0.848 <sup>0.012</sup>	0.350 <sup>0.009</sup>	32.51 <sup>2.510</sup>	1.069 <sup>0.014</sup>	0.343 <sup>0.017</sup>	10.82 <sup>0.38</sup>	---	43.90/41
Y-01-04*	55818.84	0.713 <sup>0.021</sup>	2.082 <sup>0.028</sup>	0.307 <sup>0.015</sup>	1.209 <sup>0.015</sup>	290.72 <sup>17.0</sup>	2.534 <sup>0.021</sup>	0.617 <sup>0.003</sup>	0.244 <sup>0.004</sup>	47.00 <sup>2.360</sup>	1.053 <sup>0.013</sup>	2.073 <sup>0.186</sup>	10.63 <sup>0.27</sup>	---	52.75/41
Y-01-05*	55819.20	0.753 <sup>0.013</sup>	2.062 <sup>0.015</sup>	0.302 <sup>0.009</sup>	1.220 <sup>0.008</sup>	207.75 <sup>9.50</sup>	2.547 <sup>0.028</sup>	0.576 <sup>0.011</sup>	0.226 <sup>0.007</sup>	39.16 <sup>2.450</sup>	1.058 <sup>0.015</sup>	1.514 <sup>0.187</sup>	10.89 <sup>0.23</sup>	4.876 <sup>0.085</sup>	50.13/41
Y-02-03*	55820.40	0.720 <sup>0.014</sup>	2.076 <sup>0.018</sup>	0.306 <sup>0.009</sup>	1.127 <sup>0.009</sup>	279.67 <sup>9.07</sup>	2.537 <sup>0.014</sup>	0.564 <sup>0.010</sup>	0.222 <sup>0.006</sup>	39.95 <sup>4.890</sup>	1.057 <sup>0.015</sup>	1.682 <sup>0.242</sup>	10.89 <sup>0.23</sup>	5.175 <sup>0.044</sup>	72.70/41
Y-02-00*	55821.85	0.890 <sup>0.016</sup>	1.964 <sup>0.019</sup>	0.294 <sup>0.010</sup>	1.164 <sup>0.009</sup>	63.73 <sup>3.25</sup>	2.447 <sup>0.011</sup>	0.667 <sup>0.009</sup>	0.273 <sup>0.005</sup>	38.04 <sup>2.470</sup>	1.057 <sup>0.016</sup>	0.894 <sup>0.015</sup>	10.58 <sup>0.33</sup>	4.238 <sup>0.215</sup>	58.69/41
Y-02-01*	55822.83	0.808 <sup>0.027</sup>	2.014 <sup>0.027</sup>	0.271 <sup>0.015</sup>	1.179 <sup>0.014</sup>	110.91 <sup>8.0</sup>	2.345 <sup>0.026</sup>	0.735 <sup>0.008</sup>	0.313 <sup>0.007</sup>	37.82 <sup>2.320</sup>	1.055 <sup>0.009</sup>	0.799 <sup>0.159</sup>	10.98 <sup>0.54</sup>	4.359 <sup>0.145</sup>	73.73/41
Y-02-04**	55823.81	0.975 <sup>0.027</sup>	1.871 <sup>0.025</sup>	0.265 <sup>0.011</sup>	1.189 <sup>0.013</sup>	37.45 <sup>2.31</sup>	2.341 <sup>0.024</sup>	0.699 <sup>0.002</sup>	0.299 <sup>0.003</sup>	41.02 <sup>1.971</sup>	1.058 <sup>0.071</sup>	0.541 <sup>0.005</sup>	10.91 <sup>0.15</sup>	---	28.93/38
Y-02-05**	55824.58	0.895 <sup>0.032</sup>	1.863 <sup>0.020</sup>	0.184 <sup>0.012</sup>	1.315 <sup>0.012</sup>	45.70 <sup>2.08</sup>	2.259 <sup>0.023</sup>	0.791 <sup>0.004</sup>	0.350 <sup>0.005</sup>	31.19 <sup>1.214</sup>	1.064 <sup>0.014</sup>	0.315 <sup>0.031</sup>	10.50 <sup>0.13</sup>	---	50.77/38
Y-02-02*	55825.94	1.015 <sup>0.029</sup>	1.769 <sup>0.019</sup>	0.203 <sup>0.012</sup>	1.255 <sup>0.011</sup>	25.11 <sup>1.90</sup>	2.237 <sup>0.046</sup>	0.849 <sup>0.000</sup>	0.380 <sup>0.008</sup>	37.80 <sup>1.910</sup>	1.060 <sup>0.001</sup>	0.504 <sup>0.033</sup>	10.86 <sup>0.49</sup>	3.099 <sup>0.066</sup>	67.03/41
Y-02-06*	55826.60	1.113 <sup>0.029</sup>	1.746 <sup>0.030</sup>	0.208 <sup>0.013</sup>	1.267 <sup>0.013</sup>	14.13 <sup>30.80</sup>	2.157 <sup>0.028</sup>	0.838 <sup>0.002</sup>	0.389 <sup>0.006</sup>	33.52 <sup>2.350</sup>	1.065 <sup>0.010</sup>	0.334 <sup>0.108</sup>	10.78 <sup>0.11</sup>	2.727 <sup>0.034</sup>	58.38/41
Y-03-04*	55827.33	0.943 <sup>0.025</sup>	1.793 <sup>0.026</sup>	0.132 <sup>0.015</sup>	1.261 <sup>0.014</sup>	24.52 <sup>2.67</sup>	2.085 <sup>0.028</sup>	0.857 <sup>0.010</sup>	0.411 <sup>0.011</sup>	34.59 <sup>1.650</sup>	1.060 <sup>0.008</sup>	0.339 <sup>0.095</sup>	11.01 <sup>0.24</sup>	2.672 <sup>0.012</sup>	48.70/41
Y-03-01*	55829.80	1.130 <sup>0.022</sup>	1.725 <sup>0.024</sup>	0.120 <sup>0.016</sup>	1.270 <sup>0.015</sup>	8.32 <sup>0.72</sup>	1.958 <sup>0.049</sup>	0.857 <sup>0.004</sup>	0.438 <sup>0.013</sup>	36.63 <sup>1.380</sup>	1.058 <sup>0.003</sup>	0.330 <sup>0.086</sup>	10.62 <sup>0.15</sup>	2.023 <sup>0.073</sup>	46.63/41
Y-03-05*	55830.89	1.114 <sup>0.025</sup>	1.701 <sup>0.030</sup>	0.099 <sup>0.021</sup>	1.272 <sup>0.018</sup>	7.45 <sup>0.41</sup>	1.902 <sup>0.036</sup>	0.866 <sup>0.005</sup>	0.455 <sup>0.011</sup>	39.09 <sup>2.540</sup>	1.051 <sup>0.003</sup>	0.331 <sup>0.053</sup>	11.00 <sup>0.41</sup>	---	51.52/41
Y-03-02*	55831.84	1.128 <sup>0.026</sup>	1.620 <sup>0.026</sup>	0.096 <sup>0.017</sup>	1.225 <sup>0.029</sup>	6.60 <sup>0.92</sup>	1.846 <sup>0.023</sup>	0.869 <sup>0.006</sup>	0.471 <sup>0.009</sup>	39.99 <sup>1.780</sup>	1.054 <sup>0.006</sup>	0.313 <sup>0.050</sup>	9.49 <sup>0.69</sup>	---	53.16/41
Y-03-03*	55832.81	1.200 <sup>0.025</sup>	1.629 <sup>0.020</sup>	0.096 <sup>0.013</sup>	1.222 <sup>0.011</sup>	4.89 <sup>0.31</sup>	1.934 <sup>0.029</sup>	0.852 <sup>0.008</sup>	0.441 <sup>0.011</sup>	41.39 <sup>2.970</sup>	1.063 <sup>0.009</sup>	0.321 <sup>0.110</sup>	10.70 <sup>0.58</sup>	---	34.85/41
Y-04-01*	55835.81	1.195 <sup>0.028</sup>	1.560 <sup>0.020</sup>	0.076 <sup>0.012</sup>	1.145 <sup>0.014</sup>	3.95 <sup>0.26</sup>	1.964 <sup>0.014</sup>	0.843 <sup>0.007</sup>	0.429 <sup>0.007</sup>	46.34 <sup>3.280</sup>	1.071 <sup>0.004</sup>	0.330 <sup>0.031</sup>	9.34 <sup>0.88</sup>	---	41.26/41
Y-04-02*	55836.78	1.287 <sup>0.021</sup>	1.523 <sup>0.025</sup>	0.086 <sup>0.014</sup>	1.101 <sup>0.013</sup>	3.05 <sup>0.20</sup>	1.957 <sup>0.015</sup>	0.841 <sup>0.009</sup>	0.430 <sup>0.008</sup>	46.40 <sup>1.970</sup>	1.073 <sup>0.009</sup>	0.298 <sup>0.044</sup>	9.49 <sup>0.91</sup>	1.636 <sup>0.092</sup>	34.95/41
Y-04-04*	55838.83	1.347 <sup>0.034</sup>	1.488 <sup>0.038</sup>	0.085 <sup>0.021</sup>	1.023 <sup>0.018</sup>	2.42 <sup>0.19</sup>	1.910 <sup>0.035</sup>	0.780 <sup>0.007</sup>	0.408 <sup>0.011</sup>	53.28 <sup>1.750</sup>	1.067 <sup>0.021</sup>	0.332 <sup>0.025</sup>	9.49 <sup>0.78</sup>	---	36.53/41
Y-04-06*	55840.78	1.270 <sup>0.039</sup>	1.477 <sup>0.033</sup>	0.080 <sup>0.016</sup>	0.951 <sup>0.014</sup>	3.04 <sup>0.14</sup>	1.812 <sup>0.039</sup>	0.756 <sup>0.007</sup>	0.417 <sup>0.013</sup>	49.84 <sup>2.120</sup>	1.070 <sup>0.012</sup>	0.293 <sup>0.007</sup>	8.00 <sup>0.77</sup>	---	43.20/41
Y-05-00*	55842.79	1.420 <sup>0.038</sup>	1.496 <sup>0.037</sup>	0.077 <sup>0.019</sup>	0.860 <sup>0.019</sup>	1.68 <sup>0.13</sup>	1.817 <sup>0.033</sup>	0.716 <sup>0.011</sup>	0.394 <sup>0.013</sup>	50.91 <sup>2.560</sup>	1.070 <sup>0.015</sup>	0.280 <sup>0.008</sup>	8.79 <sup>0.89</sup>	1.449 <sup>0.074</sup>	58.38/41
Y-05-01*	55843.76	1.468 <sup>0.040</sup>	1.487 <sup>0.033</sup>	0.079 <sup>0.016</sup>	0.827 <sup>0.016</sup>	1.46 <sup>0.12</sup>	1.823 <sup>0.039</sup>	0.680 <sup>0.001</sup>	0.373 <sup>0.009</sup>	53.44 <sup>2.840</sup>	1.070 <sup>0.012</sup>	0.280 <sup>0.057</sup>	9.45 <sup>0.52</sup>	---	44.12/41
Y-05-04*	55844.86	1.259 <sup>0.034</sup>	1.528 <sup>0.039</sup>	0.055 <sup>0.018</sup>	0.864 <sup>0.015</sup>	2.18 <sup>0.18</sup>	1.827 <sup>0.022</sup>	0.648 <sup>0.009</sup>	0.355 <sup>0.009</sup>	57.40 <sup>1.230</sup>	1.071 <sup>0.005</sup>	0.323 <sup>0.074</sup>	9.45 <sup>0.67</sup>	0.368 <sup>0.029</sup>	40.58/41
Y-05-06*	55847.80	1.237 <sup>0.038</sup>	1.536 <sup>0.049</sup>	0.032 <sup>0.023</sup>	0.762 <sup>0.016</sup>	1.39 <sup>0.10</sup>	1.831 <sup>0.014</sup>	0.663 <sup>0.006</sup>	0.362 <sup>0.006</sup>	61.04 <sup>2.470</sup>	1.070 <sup>0.009</sup>	0.299 <sup>0.042</sup>	8.16 <sup>0.87</sup>	---	47.60/41
Y-06-02*	55850.87	1.377 <sup>0.037</sup>	1.504 <sup>0.046</sup>	0.048 <sup>0.027</sup>	0.673 <sup>0.021</sup>	1.22 <sup>0.08</sup>	1.784 <sup>0.017</sup>	0.642 <sup>0.002</sup>	0.360 <sup>0.004</sup>	60.38 <sup>3.110</sup>	1.069 <sup>0.015</sup>	0.269 <sup>0.074</sup>	8.26 <sup>0.75</sup>	---	35.71/41
Y-07-00	55856.47	1.194 <sup>0.035</sup>	1.586 <sup>0.042</sup>	0.016 <sup>0.027</sup>	0.541 <sup>0.014</sup>	0.77 <sup>0.07</sup>	1.668 <sup>0.013</sup>	0.566 <sup>0.004</sup>	0.339 <sup>0.005</sup>	75.16 <sup>1.740</sup>	1.069 <sup>0.008</sup>	0.270 <sup>0.027</sup>	7.54 <sup>0.41</sup>	---	69.54/44
Y-08-00	55862.87	1.542 <sup>0.030</sup>	1.379 <sup>0.034</sup>	0.053 <sup>0.023</sup>	0.403 <sup>0.020</sup>	0.78 <sup>0.06</sup>	1.665 <sup>0.015</sup>	0.491 <sup>0.002</sup>	0.295 <sup>0.004</sup>	96.45 <sup>3.450</sup>	1.076 <sup>0.004</sup>	0.251 <sup>0.011</sup>	7.51 <sup>0.64</sup>	---	52.25/44
Y-08-05	55867.08	1.474 <sup>0.033</sup>	1.395 <sup>0.031</sup>	0.042 <sup>0.015</sup>	0.384 <sup>0.012</sup>	0.76 <sup>0.04</sup>	1.583 <sup>0.016</sup>	0.460 <sup>0.015</sup>	0.291 <sup>0.013</sup>	135.48 <sup>4.450</sup>	1.084 <sup>0.005</sup>	0.251 <sup>0.016</sup>	7.72 <sup>0.72</sup>	---	51.72/44
Y-09-02	55871.06	1.649 <sup>0.032</sup>	1.399 <sup>0.040</sup>	0.038 <sup>0.037</sup>	0.318 <sup>0.026</sup>	0.40 <sup>0.06</sup>	1.530 <sup>0.013</sup>	0.457 <sup>0.012</sup>	0.299 <sup>0.011</sup>	162.37 <sup>7.870</sup>	1.084 <sup>0.012</sup>	0.250 <sup>0.007</sup>	7.76 <sup>0.83</sup>	---	65.29/44
Y-10-01	55877.63	1.612 <sup>0.046</sup>	1.481 <sup>0.032</sup>	0.020 <sup>0.024</sup>	0.296 <sup>0.016</sup>	0.34 <sup>0.05</sup>	1.486 <sup>0.018</sup>	0.422 <sup>0.002</sup>	0.284 <sup>0.006</sup>	199.24 <sup>4.510</sup>	1.089 <sup>0.009</sup>	0.258 <sup>0.002</sup>	7.57 <sup>0.65</sup>	---	64.36/44

X=96371-03 and Y=96438-01 are the prefixes of observation Ids. Blank lines mark transitions between different spectral states.

\* Spectra are fitted with additional Gaussian lines of energy  $\sim 6.5$  keV, and \*\* spectra are fitted with an additional LAOR component with TCAF model.

$T_{in}$ , and  $\Gamma$  values indicate combined DBB and PL model fitted DBB temperatures in keV and PL photon indices respectively.

$\dagger$  DBBf, PLf represent combined DBB and PL model fitted fluxes in 2.5-25 keV band for DBB and PL model components respectively in units of  $10^{-9} \text{ ergs cm}^{-2} \text{ s}^{-1}$ .

$\dot{m}_h$  (in Eddington rate unit),  $\dot{m}_d$  (in Eddington rate unit),  $X_s$  (in units of Schwarzschild radius), and  $R$  are TCAF fitted Keplerian disk, sub-Keplerian halo, shock location and compression ratio values respectively. Norm. and  $M_{BH}$  are TCAF fitted normalization and BH mass values respectively.

$\dagger\dagger$  Frequencies of the dominating QPO in Hz are mentioned. DOF means degrees of freedom of the spectral model fits.

The values of  $\chi^2$ , and DOF of TCAF model fitted spectra are mentioned in Col. 16. The ratio is the  $\chi^2_{red}$ .

Note: average values of 90% confidence  $\pm$  values obtained using 'err' task in XSPEC, are placed as superscripts of fitted parameter values.

## Appendix II

Combined LAOR plus TCAF Spectral Fitted LAOR Parameters

obs. Id	MJD	Line Energy (keV)	Index	$R_{in}$ ( $r_g$ )	$R_{out}$ ( $r_g$ )	Inclination (Degree)	LAOR Norm.
(1)	(2)	(3)	(4)	(5)	(6)	(7)	(8)
X-03-00	55806.51</						